Landslides (2023) 20:1667–1678
DOI 10.1007/s10346-023-02070-2
Received: 29 November 2022
Accepted: 12 April 2023
Published online: 13 May 2023

Xuemei Liu · Pengcheng Su · Yong Li · Zhaoxu Xia · Siyuan Ma · Rui Xu · Yao Lu · Dahu Li · Heng Lu · Renmao Yuan

Spatial distribution of landslide shape induced by Luding *Ms*6.8 earthquake, Sichuan, China: case study of the Moxi Town

Abstract Landslides induced by the 2022 Luding *Ms* 6.8 earthquake mainly occurred in the Moxi Town, the Detuo Town, and the Wanggangping County, causing serious casualties and property losses. Among these places, the Moxi Town is the nearest one to the earthquake epicenter, where the landslides triggered by the Luding earthquake are not huge but with distinctly different shapes. Based on field investigation, the shapes of landslides are identified and can be categorized into 9 types (e.g., wide shape, strip, vertical rectangle, horizontal rectangle, water drop, fan, Y shape, sporadic, and knife shape), which are influenced mainly by 8 influencing factors, including land use type, lithology, slope, slope style, aspect, elevation, starting position, and watershed evolution index. According to the statistical analysis results, lithology could be the main factor causing the different shapes of landslides. Landslides with the wide shape are more likely to occur in the looser gravel layer. The long and narrow landslides with the strip shape are more likely to occur in the granite formation, the moving direction of which is affected mainly by fractures in the rock mass. In the same lithology, the shapes of landslides are affected mainly by the slope, the elevation, and the original position. The distribution characteristics of different landslide shapes could be used to investigate the influences of the local terrain, lithology, and other factors. At the same time, landslide shapes can reflect the landslide evolution, which provides essential support on the emergency response and risk mitigation.

Keywords Luding *Ms*6.8 earthquake · Landslide induced by earthquake · Shape of landslide

Introduction

On September 5, 2022, the Luding *Ms* 6.8 earthquake occurred in the Luding county, Sichuan province of China, the epicenter of which is located in the Moxi Town (29.59° N, 102.08° E), and the seismogenic fault of which is the Moxi fault. Field investigation showed that the coseismic landslides are distributed mainly around the epicenter area, including the Moxi Town, Detuo Town, and Wanggangping County, or along the Moxi fault, suggesting that the earthquake energy is released concentratedly near the epicenter and along the fault. Although most of the coseismic landslides triggered by this earthquake are not huge, they still caused serious casualties and property losses (Fan et al. 2022; Xiao et al. 2023). The Moxi Town is the nearest one to the epicenter, where coseismic landslides show obviously different shapes with a certain spatial distribution characteristic. The landslide shapes could reflect the landslide evolution, such as their expansion direction. Here, the study region is only in the Moxi Town with a relatively small area, being located in the same seismic intensity zone (VII) and peak ground acceleration area (0.3 g) (China Seismological Bureau, Ministry of Emergency Management 2022. 9), where the precipitation rate also is similar; therefore, the conditions of earthquake energy and rainfall are considered unchanged in the study area. It thus inferred that the difference of landslide shapes can reflect the different basic background settings, such as terrain, landform, lithology, and land use type. In this study, the spatial distribution characteristics of landslide shapes in the Moxi Town were discussed first, and the causes of them were then analyzed. The results can be used for explaining the influence of topographic, lithology, and other background factors on seismic amplification and provide a reference for risk assessment of coseismic landslides (Huang et al. 2008; Xu 2009, Xu et al. 2009; Xu and Li 2010).

Study area

The Moxi Town is located in the east of the Gongga Mountain and in the northeast of the Moxi fault, with the height difference of over 1 km. The central part of this area is flat, the southeast area is relatively lower, and the other places are surrounded by hills or mountains. In the study area, the main river (Yajiagan River) runs from northwest to southeast, connecting with the Yanzigou Valley, Mozigou Valley, and Hailuogou Valley in the west. They converged at the southeast corner of the Moxi Platform and runs into the Moxi River, which finally flows into the Dadu River. The Moxi Platform is seated between Xinxing Town and Moxi Town with a height difference of about 120 m, which is about 10 km long and 1 to 2 km wide (Zheng 2001; Zhang et al. 2013; Li et al. 2010; Ma et al. 1994). The sediments in the Moxi Platform consist of glacial/glacial water sediments and debris deposits from the Last Glacial period to the Holocene. Most of them came from the Swallow Gully, the Mozi Gully, and the Conch Gully. The terraces on both sides of the platform can be divided into four levels (Zheng 2001). The study area includes part of the Moxi Platform, mainly being composed of quaternary glacial looser gravel layer, and the mountains around the platform, mainly being composed of granite. The whole study area is about 5 km long and 2 km wide with about 7 km from the epicenter (Figs. 1 and 2).

Field investigation showed that the landslides induced by this earthquake are mainly distributed along rivers and roads. Although the landslides are not huge, most of the roads along the mountains were destroyed by landslides, which caused some casualties and seriously affected the emergency rescue work (Fig. 3) (Fan et al. 2022; Huang et al. 2022).

The landslide shapes are formed by the combined action of earthquake energy and the factors such as topographic, lithology and others, which can reflect the evolution of landslide.

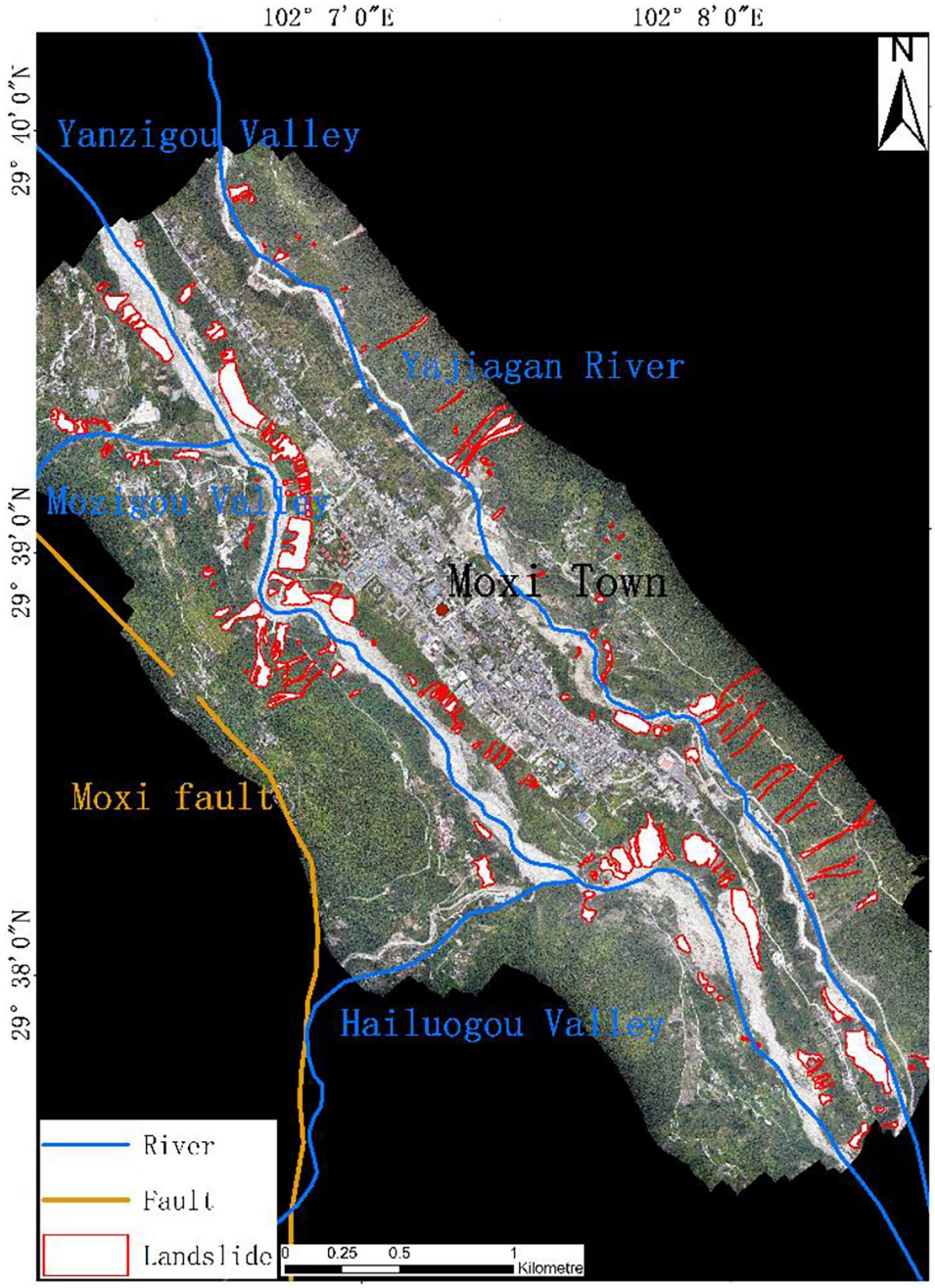

Fig. 1 Spatial distribution of landslides in the study area

Susceptibility assessment of landslides with different shapes can provide a reference for emergency disaster prevention in the early times after earthquake. (Luo and Wang 2013; Zhang 2012; Xu 2009a; Xu 2009b; Xu and Li 2010; Jibson 2007; Makdisi and Seed 1978; Liu et al. 2013; Huang and Xu 2008; Oji et al. 2009; Chigira et al. 2010; Marc et al. 2016; Mahdavif and Solaymani 2006; Li et al. 2010).

Landslide characteristics

The 7-cm-resolution unmanned aerial vehicles (UAV) image data on September 7, 2022, in the study area, supplied by Chengdu Zongheng Dapeng UAV Technology Co., Ltd. was used to interpret the landslides. The interpretation results were verified and corrected by field survey results (Fig. 4).

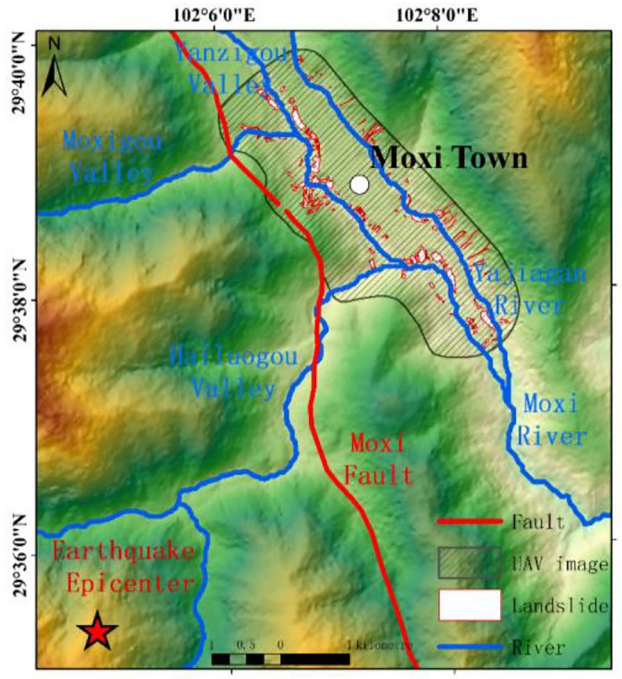

Fig. 2 The epicenter of the Luding earthquake and UAV image of study area

As it is shown in Fig. 4a, the zone a is identified as landslide on the image, but actually, it is the river beach gravel (Fig. 4a). While the zone a in Fig. 4b is not as large as it presented in the UAV image, because some old landslides are distributed around the new one. In Fig. 4c, the zone a and zone b are shaded by plants, the boundary of these landslides is thus not clear, which can be clarified based on the field survey results. In zones c, d, e, f, and g in Fig. 4c, landslide sources are developed near the hill foot and mixed with river beach sand gravel, resulting in a difficult to distinguish landslide boundary. The zones a, d, c, d, and e in Fig. 4d are narrow and long; the boundaries of these landslides are also unclear because of the influence of plants. The photos of these landslides thus were taken from different sides during field investigation to clarify their boundaries. After being verified and corrected, there are 192 co-seismic landslides in the study area with a total area of 38.6×10^4 m^2. The scale of these landslides in the study region is relatively small but with obviously different shapes and a certain spatial distribution characteristic.

Characteristics of landslide shapes

In the study, the shape of the landslide only refers to the geometric shape being outlined on the covered area of the landslide. The landslide shapes can be classified into 9 types, as shown in Fig. 5. The landslides with the sheet and strip shapes are the two principle types in this region. Other shapes include the shapes of the vertical rectangle, horizontal rectangle, water drop, fan, Y shape, sporadic, and knife.

Statistical results of number and area showed that the number of sporadic landslides is the largest among the 9 shapes, followed by the strip, water drop and vertical rectangle landslides (Fig. 6), which suggested that the landslide features of large number but small scale. The sheet landslides with very large covering area but small in number (Figs. 6 and 7). The numbers and areas of strip, water drop and vertical rectangle landslides are at a medium level.

Fig. 3 Landslide hazards induced by the Luding earthquake in the Moxi Town (September 11 to 15, 2022)

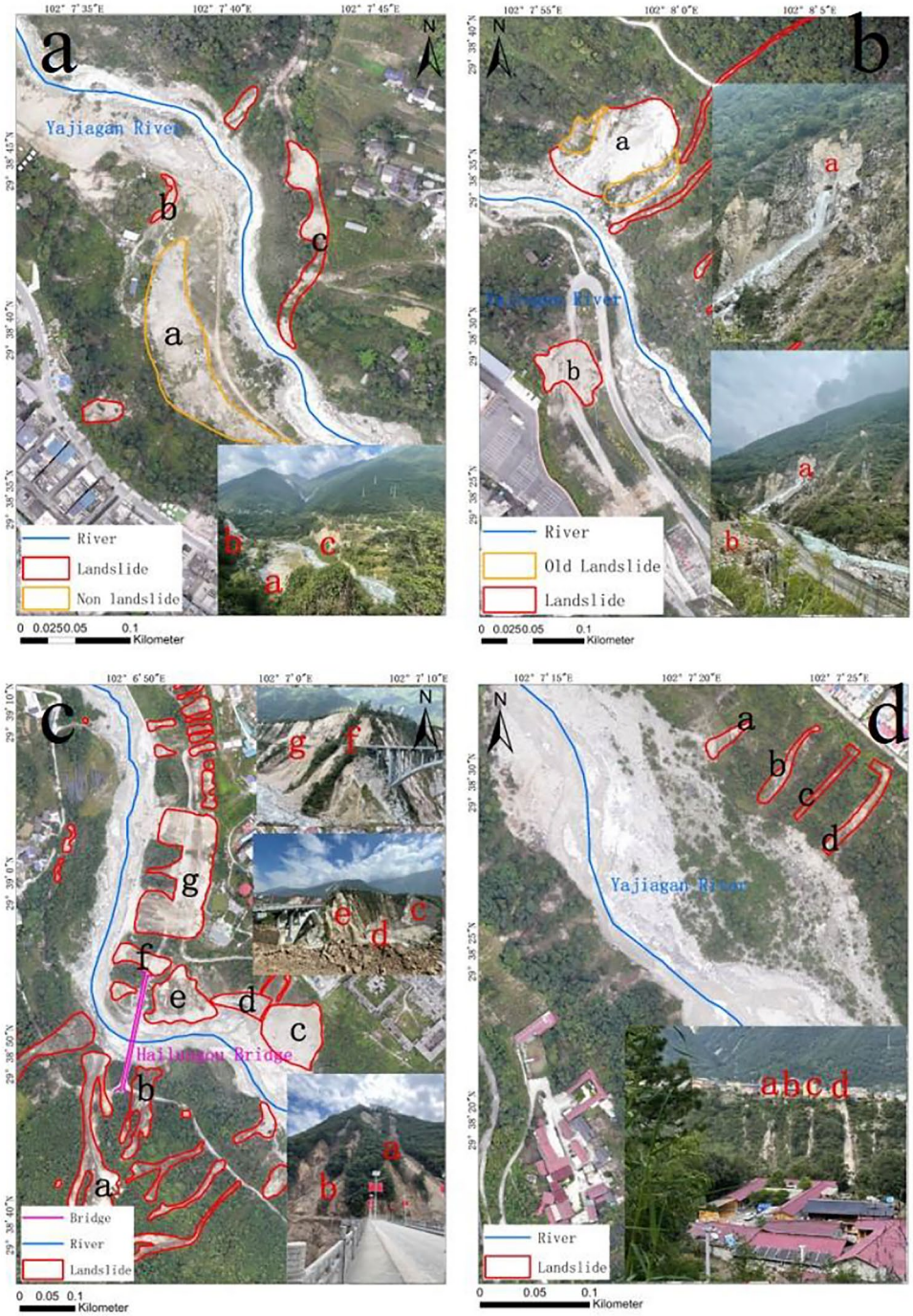

Fig. 4 Landslide spatial distribution and shapes

Here, 8 background factors of the landslide shapes in the study area are further analyzed, including the land use type, lithology, slope, slope style, aspect, elevation, starting position, and watershed evolution index.

Among them, the land use type can be classified into 12 categories, including forest, river, ditch, farmland, road, residence, between river and residence, between river and farmland, between river and road, between river and ditch, between road and bridge, and between farmland and road. The statistical results show that landslides are mainly located near the river, between river and residence, between river and road, and between river and farmland. In particular, the sheet landslides are mainly located between river and farmland and between river and road. The strip landslides are mainly located near the road. The water drop landslides are mainly located between river and residence and between river and road. The vertical rectangular landslides are located between road and farmland. The Y shape landslides are mostly located between road and bridge.

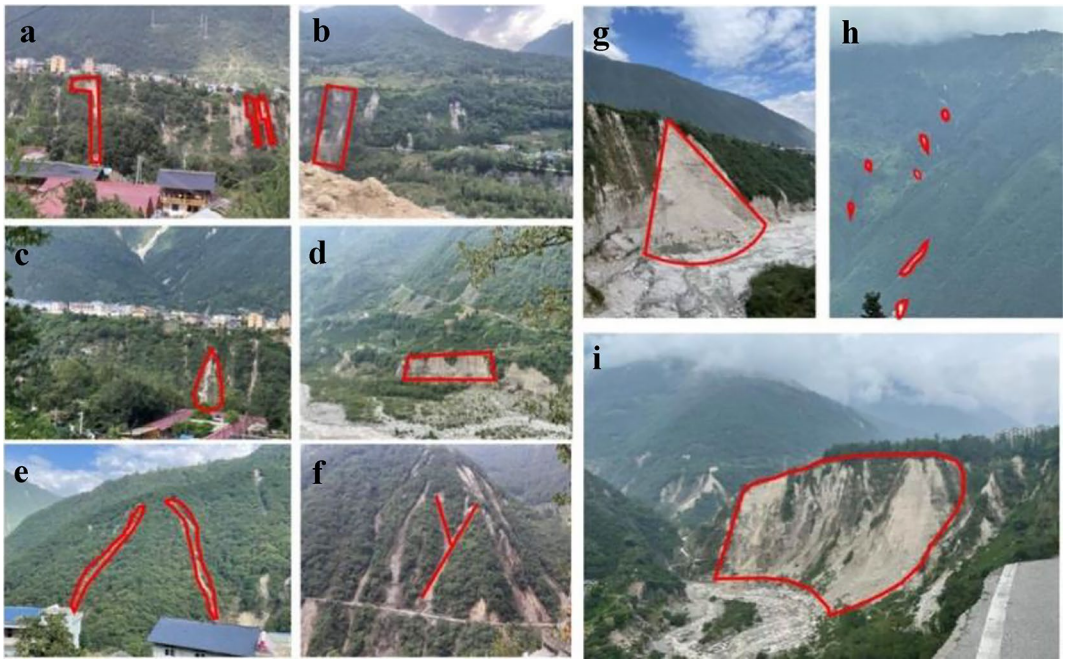

Fig. 5 Nine shapes of landslides in the study area **a** knife, **b** vertical rectangle, **c** water drops, **d** horizontal rectangle, **e** strip, **f** Y shape, **g** fan, **h** sporadic, **i** sheet

The sporadic landslides are scattered between road and ditch. The fan landslides are located near the river, between river and road. The knife landslides are mainly between river and residence (Fig. 8).

The lithologies are mainly loose gravel layer and granite in the study area (Fig. 9) (Chen et al. 2011; Lanbin Shi and Chuanyong Lin 1992; Yang and Hongtai 2013), which is the main materials of landslides. According to the statistical results, the knife, sheet, fan, water drop, horizontal rectangle and vertical rectangle landslides are mostly located in the loose gravel layers. The Y shape and strip landslides are mainly occurred in the granite mountains on both sides of the Moxi Platform. Half of the sporadic landslides occurred in the loose gravel layer and half in the granite area (Fig. 10).

In order to analyze the influence of topographic on the landslide's shapes, the slope type, landslide starting position, elevation, slope, aspect, and basin hypsometric index of each landslide shape were counted (Fig. 11). Statistical results show that the fan, water drop, and Y shape landslides are mostly located on concave or convex slopes. The half of sheet and strip landslides occurred in the concave or convex slopes and half in the flat slopes. For the sporadic landslides with small scales, it is difficult to distinguish the slope types, although the results show that they are mostly located on a flat slope. The knife, horizontal rectangle, and vertical rectangle landslides are mostly located on the flat slope.

Statistical results of landslide original positions show that knife, sheet, and fan shape landslides almost start from the upper part of slopes. Most of the horizontal rectangle and vertical rectangle starts from the upper part of slopes, and a few of them starts from the middle part of slopes. By contrast, most of the water drop and strip landslides start from the middle of slopes, and a few of them starts from the upper part of the slope. The Y shape landslides almost start from the middle of the slope. However, the sporadic landslides can originally occur at all three parts of slopes (Fig. 12).

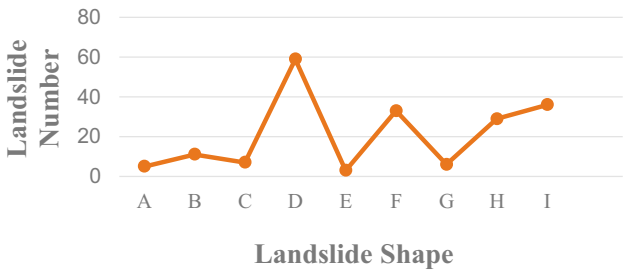

Fig. 6 Numbers of landslides with different shapes in the study area **a** knife, **b** sheet, **c** horizontal rectangle, **d** sporadic, **e** fan, **f** water drops, **g** Y shape, **h** vertical rectangle, **i** strip

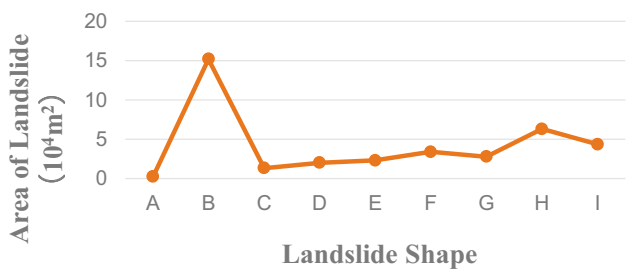

Fig. 7 Areas of landslides with different shapes in the study area **a** knife, **b** sheet, **c** horizontal rectangle, **d** sporadic, **e** fan, **f** water drops, **g** Y shape, **h** vertical rectangle, **i** strip

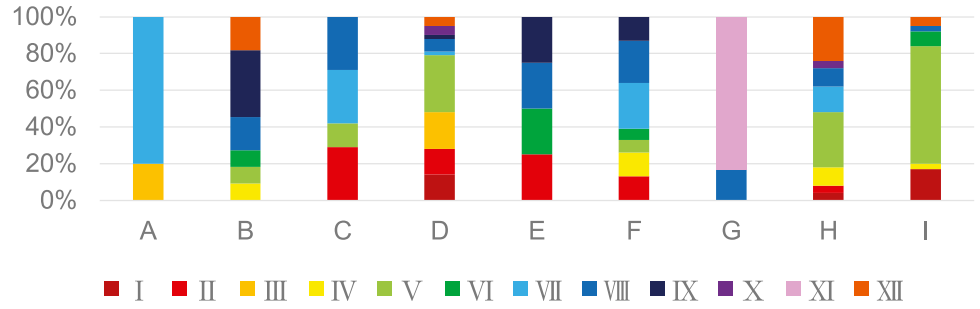

Fig. 8 Landslides in the different land use areas **a** knife, **b** sheet, **c** horizontal rectangle, **d** sporadic, **e** fan, **f** water drops, **g** Y shape, **h** vertical rectangle, **i** strip (I forest, II river, III ditch, IV farmland, V road, VI residence, VII between river and residence, VIII between river and road, IX between river and farmland, X between river and ditch, XI between road and bridge, XII between farmland and road)

Fig. 9 Landslides with different lithologies in the study area **a** loose gravel layer, **b** granite

Based on the statistical results of elevation (Fig. 13), it shows that positions of the water drop landslides are relatively lower, mainly from 1200 to 1500 m. The sheet, horizontal rectangle, fan, vertical rectangle, and sporadic landslides occurred mainly on the elevations from 1300 to 1600 m, which are higher than that of the water drop landslides. The knife landslides developed the lever between 1500 and 1700 m. The elevation of Y shape and strip landslides is mainly from 1500 to 1800, which is the highest compared with that of other landslide types.

For slope angle, statistical results show that landslides in the study area range from 30 to 50°. The slopes with the sheet, Y shape, and strip landslides are the largest exceeding 60°. The slopes with the horizontal rectangle landslides are relatively smaller between 10 to 30°. The slopes with the drop and sporadic landslides range from several degrees to 60° (Fig. 14).

The aspects of slopes with the knife, sheet, sporadic, water drop, vertical rectangle, and strip landslides mostly are the southwest and west. The aspects of slopes with the horizontal rectangle and fan landslides are mainly southeast. The Y shape landslides are mainly located on the north faces (Fig. 15). In the whole study area, the aspects of slopes are mainly southeast (Fig. 16).

The basin hypsometric index is a quantitative description of the geomorphic development stage. The different levels of which reflected the different basin evolution stages and have different influences on landslides (Singh et al. 2008; Altin and Gökkaya 2015; Li et al. 2006; Xiang et al. 2015). In this study, the fluctuation ratio method (Formula 1) is used to calculate the basin hypsometric index (Chang et al. 2015), as following:

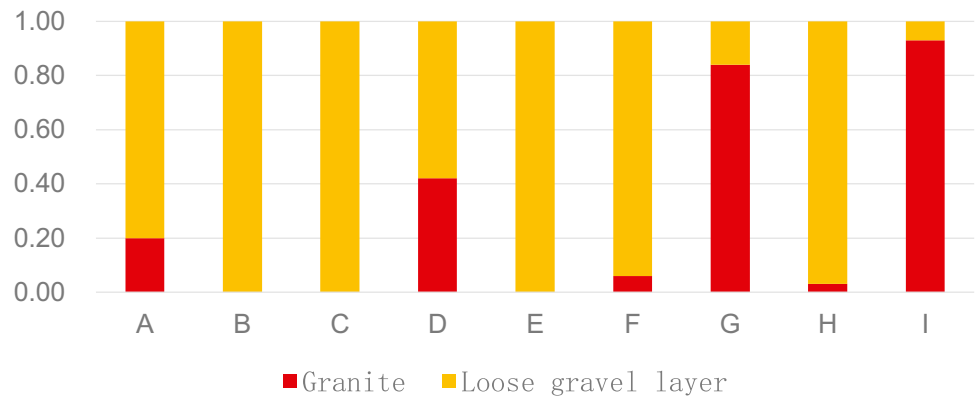

Fig. 10 Statistical results of landslides in different lithologies **a** knife, **b** sheet, **c** horizontal rectangle, **d** sporadic, **e** fan, **f** water drops, **g** Y shape, **h** vertical rectangle, **i** strip

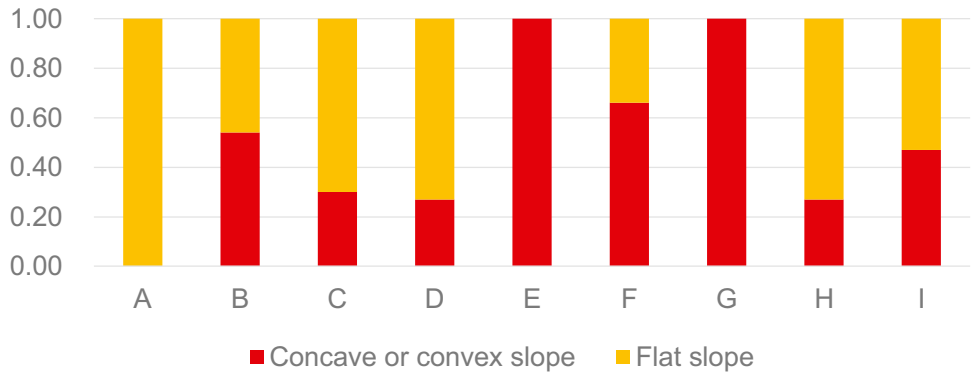

Fig. 11 Landslides on different slope types **a** knife, **b** sheet, **c** horizontal rectangle, **d** sporadic, **e** fan, **f** water drops, **g** Y shape, **h** vertical rectangle, **i** strip

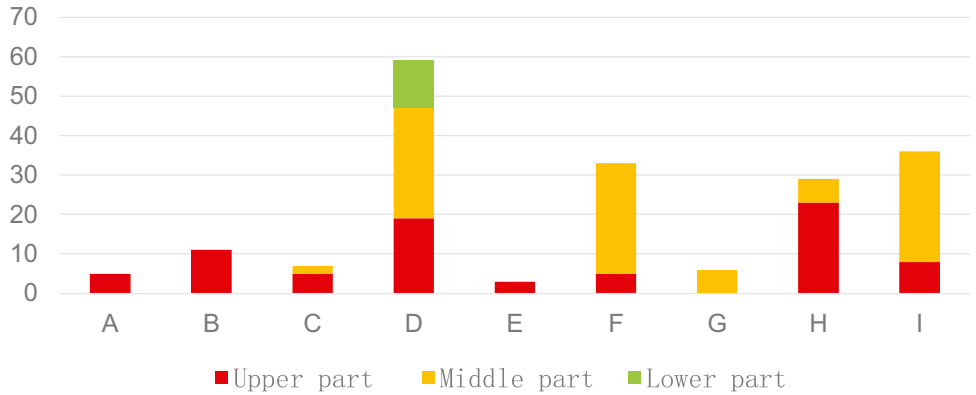

Fig. 12 Start positions of landslides with different types **a** knife, **b** sheet, **c** horizontal rectangle, **d** sporadic, **e** fan, **f** water drops, **g** Y shape, **h** vertical rectangle, **i** strip

$$\mathrm{HI} = \frac{\mathrm{EL}_{avg} - \mathrm{EL}_{min}}{\mathrm{EL}_{max} - \mathrm{EL}_{min}} \quad (1)$$

where HI represents the basin hypsometric index, EL_{avg} is the average elevation, EL_{min} represents the minimum elevation, and EL_{max} represents the maximum elevation.

The basin hypsometric index is between 0.4 and 0.6, indicating the prime geomorphic development stage of the basin. The basin evolution index is less than 0.4, indicating that the geomorphic development of the basin is in old age. The index is larger than 0.6, suggesting that the basin is in juvenile stage (Strahler et al. 1952; Li et al. 2006; Xiang et al. 2015; Chang

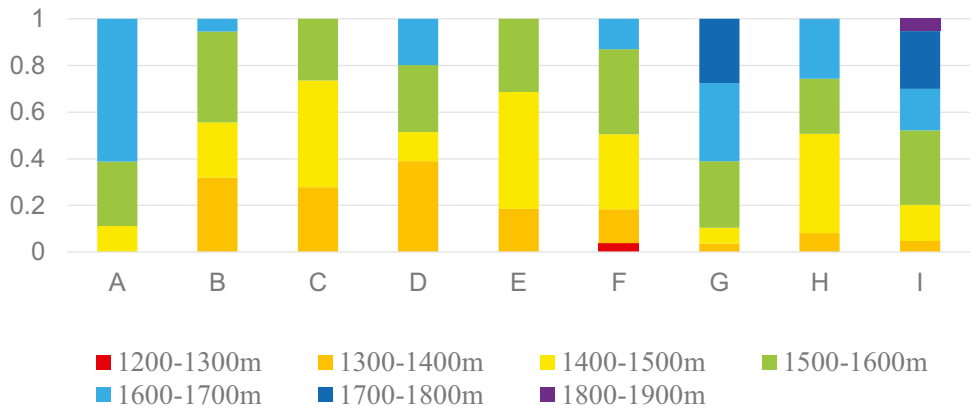

Fig. 13 Elevations of landslides with different types **a** knife **b** sheet, **c** horizontal rectangle, **d** sporadic, **e** fan, **f** water drops, **g** Y shape, **h** vertical rectangle, **i** strip

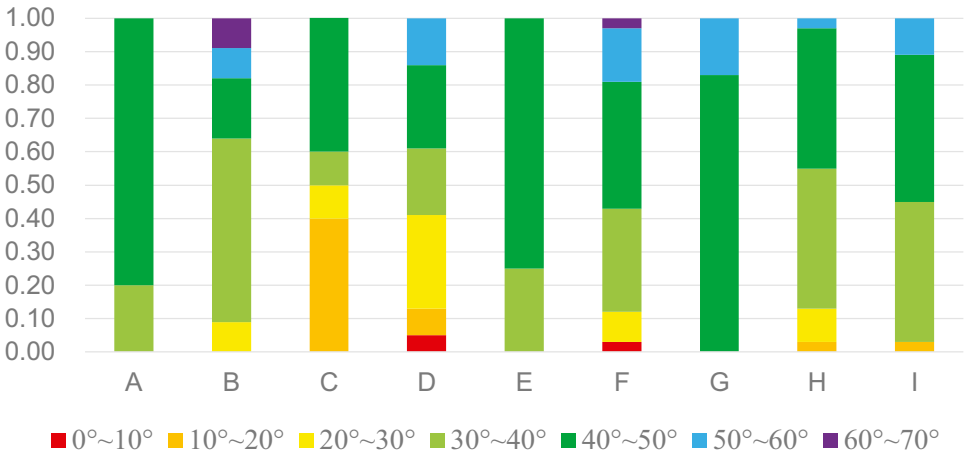

Fig. 14 Slope angles of landslides with different types **a** knife, **b** sheet, **c** horizontal rectangle, **d** sporadic, **e** fan, **f** water drops, **g** Y shape, **h** vertical rectangle, **i** strip

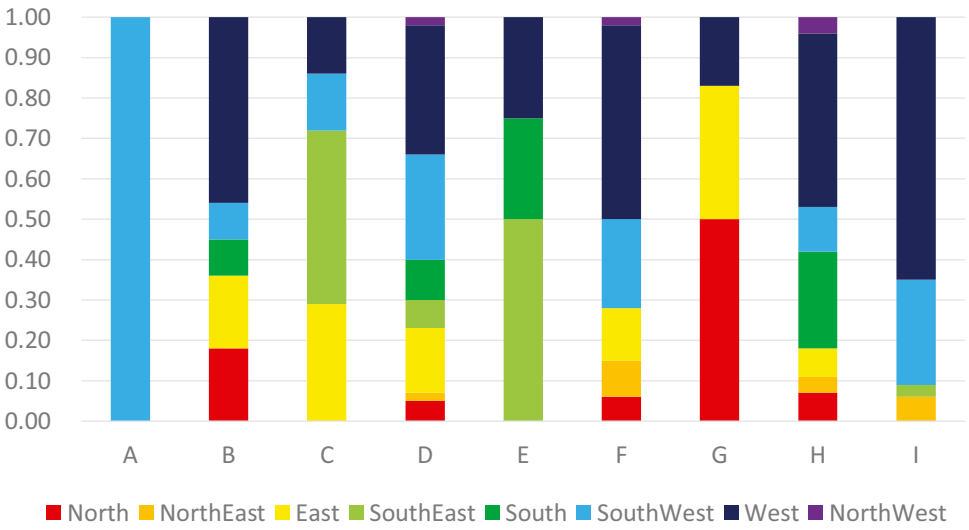

Fig. 15 Aspects of slopes with different landslide types **a** knife, **b** sheet, **c** horizontal rectangle, **d** sporadic, **e** fan, **f** water drops, **g** Y shape, **h** vertical rectangle, **i** strip)

et al. 2015). The study area is located at the intersection of six basins, where the basin hypsometric indexes range about from 0.48 to 0.5 (Fig. 17). It means that all the basins related to the study area are in the prime age, which are more prone to induce landslide.

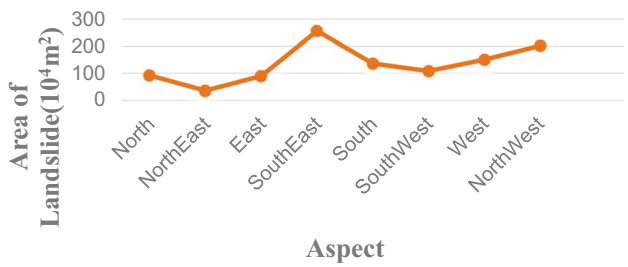

Fig. 16 Aspects of different landslide types in the study area

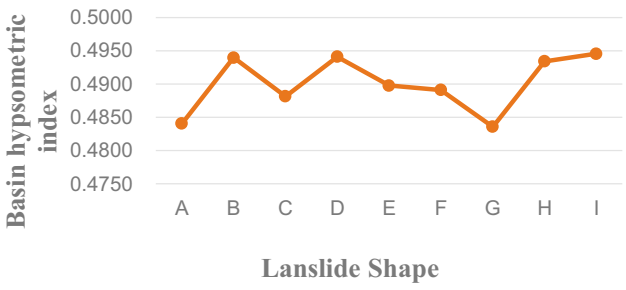

Fig. 17 Hypsometric indexes of landslides **a** knife, **b** sheet, **c** horizontal rectangle, **d** sporadic, **e** fan, **f** water drops, **g** Y shape, **h** vertical rectangle, **i** strip

Susceptibility assessment of landslides with different shapes

In this study, the information value model is used to assess the susceptibility of the landslides with these 9 shapes. Information value model is a statistical method based on the probability theory, according to the relationship between influence factors and landslides to analyze the likelihood of landslide occurrence. ArcGIS reclassify tools are used to classify each factor and calculate information values by the formula as following:

$$Iij = \ln \frac{ALij/Ai}{AL/A} \quad (2)$$

where I represents information value. i represents the ith impact factor (e.g., land use type, lithology, slope type, slope, aspect, elevation, starting position, and basin evolution index) of landslide. I_{ij} represents the jth grade of the ith impact factor (e.g., loose gravel layer and granite of lithology). AL_{ij} represents the total area of

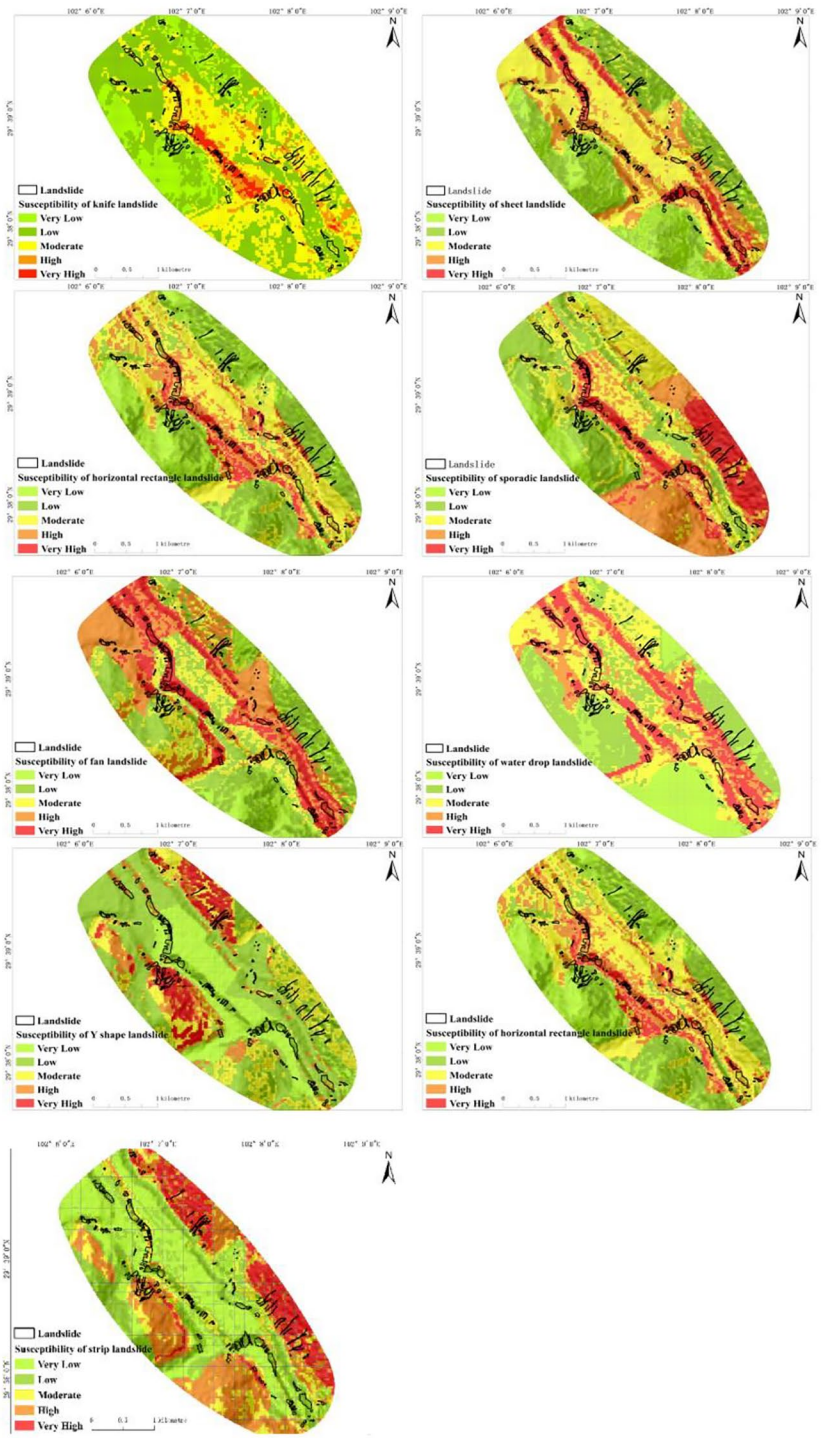

Fig. 18 Susceptibility assessment of landslides with nine shapes

landslides occurred in the *j*th grade of the *i*th impact factor. A_i represents the total area of the *i*th impact factor in this study region. AL represents the total area of landslides in the study region. *A* represents the total area of the study region (Yang et al. 2022; Che et al. 2012; Ba et al. 2018; Sharma et al. 2015; Deng et al. 2014).

The information value represents the contribution of the influence factor on inducing landslide. The information values of all influence factors are superposed as the landslide's susceptibility values. The larger the value is, the higher susceptibility of landslide will be (Ba et al. 2017; Pasang and Kubicek 2018; Keefer 2000; Chen et al. 2016).

The susceptibility values of the landslides with 9 shapes are shown in Fig. 18. The susceptibility assessment results show that the knife landslides are mostly located between river and road, where the high susceptibility area of the knife landslides is small and is mainly distributed between Mozi Valley and Hailuogou Valley. The sheet landslides are mainly developed in the loose gravel layer between rivers and roads, where the area of high susceptibility is larger than that of the knife landslide area. The water drop landsides also are located mainly in the loose gravel layer between rivers and roads, the susceptibility features of which are similar to that of the sheet landslides.

The horizontal rectangle landslides are distributed on both sides of the river near the intersection of the Yanzigou Valley and Hailuogou Valley. The susceptibility zones of the sporadic landslides are distributed on the granite mountains along both sides of the Yajiagan River. Similarly, the susceptibility regions of the fan landslides are distributed between river and road. While the Y shape landslides are distributed on the granite mountains between road and bridge. The vertical rectangle landslides are distributed between different rivers. The strip landslides are mainly distributed on the granite mountains in the northeast of the Yajiagan River.

Discussion and conclusions

In this study, according to the length and width ratio of landslide shapes, and the scale of the landslides, 9 landslide shapes can be further regrouped into three categories, which is helpful for discussing the relationship between landslide shapes and impact factors. The first category is the wide landslide with about 1 of the length and width ratio, including the sheet, vertical rectangle, horizontal rectangle, and fan shape landslides. The second category is the long and narrow landslides, the length and width ratio of which is more than one. This category includes the Y shape and strip landslides. The third category is small-scale landslides, including the sporadic, knife, and water drop landslides.

The loose gravel layer between river and road is the high susceptibility region for the wide landslides. Based on the field survey, the gravel layer in this area is loosely accumulated materials, which provides the conditions for collapsing. Compared to hard rock layer, loose gravel layer has an obvious amplification effect on seismic waves, which increases with earthquake energy increasing.

The sliding direction of landslides caused by the earthquake is highly correlated with the propagation direction of seismic wave. The main sliding direction of earthquake-induced landslide is opposite to the propagation direction of seismic wave. After the load of seismic wave exceeds the stability limit of slope, the load is released in the opposite direction of seismic wave, occurring the landslide in the opposite direction. As the earthquake energy along the fault is attenuated perpendicular to the strike of fault, the direction of landslide is probably perpendicular to the fault as well. In the study area, the strike of the Moxi fault is near the south, and the attenuation direction of earthquake energy is eastward. Impacted by the earthquake energy, the wide landslides are thus mainly on the west slope (Xu et al., 2009b; Huang et al. 2008; Oji et al. 2009; Chigira et al. 2010; Marc et al. 2016), which are caused by the earthquake energy acting on the loose gravel layer. Among the different wide landslides, the scale of the sheet and fan landslides are larger than that of the vertical rectangle and horizontal rectangle landslides. The start position and elevation of the sheet and fan landslides are higher than that of the vertical rectangle and horizontal rectangle landslides; therefore, there is enough space for forming large-scale landslides. According to the above analysis, it can be concluded that lithology is principle one of the factors to induce wide landslides, the start position and elevation controlled the scale of wide landslide. More important, the landslides with high start position and elevation are likely to run a long distance. It suggests that attention should be paid not only on the place where landslide occurs, but also on the surrounding area of the landslide point.

The granite mountains between road and bridge are the high susceptibility region for the Y shape and strip landslides with the long and narrow features. According to the field survey, this category of landslides is mainly in the broken granite region. The seismogenic fault (the Moxi fault) of the Luding earthquake is a branch of the Xianshuihe fault zone. Because of extrusion of the Xianshuihe fault zone in geological history, the rock mass along the fault is strongly broken with poor geotechnical properties, producing many fracture zones with the different width from tens of meters to several kilometers along the fault zone. In fact, many ancient or history landslides have been caused by severe activity (earthquake) or creep slipping along the Xianshui fault. The structures in the rock mass play a controlling role for landslide occurring (Guo et al. 2015; Tan-yu et al. 2010; Li et al. 2014). In the study area, the directions of the Y shape or serpentine strip landslides are also influenced by the direction of rock fractures, which are mainly located on the high elevation and steep slope, mostly occurred in concave-convex slope and started from the middle of slopes. It thus can be concluded that the long and narrow landslides are mainly influenced by the local terrain and lithology, and the directions of landslides are mainly controlled by the fracture directions in the rock mass. Therefore, the long and narrow landslides in granite mountain areas are likely to be developed along the direction of rock fractures, more attention should be paid on the direction of rock fractures during field investigation.

The knife and water drop landslides with small scales are mainly distributed between the river and farmland, and between the road and residence. The slope and elevation of this category landslides are lower with short distance from the starting position to the bottom, there thus is no enough space to form large scale landslides. Landslide materials were only accumulated at the slope bottom, forming the shape like water drop with the feature of narrow upper and wide lower. The elevations of knife landslides are slightly higher than that of water drop landslide. The starting positions of knife landslide are mostly at the upper part of slopes, but the sliding-down force of small-scale landslide is insufficient to push the landslide materials to the bottom, it

often formed the like shape knife with the feature of the wide upper and narrow lower. For this category landslides, the scale of landslides could be impacted by the land use type, the shapes of which are impacted by the start position, elevation, and slope.

Field investigation for future earthquakes in the same region, the susceptibility analysis results presented in this study can supply some useful information on identifying the places where are prone to large-scale landslides and the regions where wide landslides are easy to occur. For the wide landslides, more attention needs to be paid on the landslide lateral coverage. While for the long and narrow landslides, the direction of rock fractures should be the focus of investigation.

In summary, the terrain, lithology, and other factors impact the landslide shapes. Among them, lithology is the main factor that caused the different landslide shapes in this region. Under the same earthquake condition, the looser gravel layer is more likely to induce the wider landslides, the granite is more likely to produce the longer and narrower landslides. In the area with the same lithology, the landslide shape is mainly impacted by the slope, elevation, and the start position. The susceptibility of the landslides with different shapes could be assessed base on the topography, geomorphology, and geological factors in this region. The landslide shapes could reflect the landslide evolution and provide essential support for emergency response and risk mitigation.

Funding

The research reported in this manuscript is funded by the Strategic Priority Research Program of the Chinese Academy of Sciences (Grant No. XDA23090202) and the National Nonprofit Fundamental Research Grant of China, Institute of Geology, China Earthquake Administration (Grant No. IGCEA2202) and the Youth Key Projects of Earthquake Emergency and Information (Grant No. CEAEDEM202316).

Data availability

The Luding earthquake landslide shape elements are available at https://zenodo.org/record/7860906#.ZEdHsYRBzX4.

Declarations

Competing interests The authors declare no competing interests.

References

Altın TB, Gökkaya E (2015) Landslide-triggering factors in Korucak Subbasin, North Anatolian, Turkey. Procedia Earth and Planetary Sci 15:566–572

Ba Q, Chen Y, Deng S, Wu Q, Yang J, Zhang J (2017) An improved information value model based on gray clustering for landslide susceptibility mapping. ISPRS Int J Geo Inf 6(1):18

Ba Q, Chen Y, Deng S, Yang J, Li H (2018) A comparison of slope units and grid cells as mapping units for landslide susceptibility assessment. Earth Sci Inf 11(3):373–388

Chang ZY, Wang J, Bai SB, Zhang ZG (2015) Comparison of hypsometric integral methods. J Arid Land Resour Environ 29(3):171–175

Che VB, Kervyn M, Suh CE, Fontijn K, Ernst GGJ, del Marmol M-A, Jacobs P (2012) Landslide susceptibility assessment in Limbe (SW Cameroon): a field calibrated seed cell and information value method. Catena 92:83–98

Chen GH, Min W, Song FM, Jiao DC, Xu HT (2011) Preservation of coseismic surface rupture in different geomorphological settings from the study of the 1786 Moxi earthquake. Seismol Egol 33(4):804

Chen T, Niu R, Jia X (2016) A comparison of information value and logistic regression models in landslide susceptibility mapping by using GIS. Environ Earth Sci 75(10):1–16

Chigira M, Wu X, Inokuchi T, Wang G (2010) Landslides induced by the 2008 Wenchuan earthquake, Sichuan, China. Geomorphology 118:225–238

Deng H, He Z, Chen Y, Cai H, Li X (2014) Application of information quantity model to hazard evaluation of geological disaster in mountainous region environment: a case study of Luding County, Sichuan Province. J Nat Disasters 23(2):67–76

Fan X, Wang X, Dai L, Fang C, Deng Y, Zou C, Xu Q (2022) Characteristics and spatial distribution pattern of MS6.8 Luding earthquake occurred on September 5, 2022. J Eng Geol 30(5):1504–1516

Guo CB, Du YB, Zhang YS, Zhang GZ, Yao X, Wang K, Liu J (2015) Geohazard effects of the Xianshuihe fault and characteristics of typical landslides in western Sichuan. Geol Bull China 34(1):121–213

Huang R, Xu Q (2008) Catastrophic landslides in China. J Eng Geol

Huang RQ, Pei X, Li T (2008) Kinetics charateristics of large landlides triggered by May 12th Wenchuan earthquake. J Eng Geol 16(6):721–729

Huang Y, Xie C, Li T, Xu C, He X, Shao X, Chen Z (2022) An open-accessed inventory of landslides triggered by the MS 6.8 Luding earthquake, China on September 5, 2022. Earthquake Res Adv 100181

Jibson RW (2007) Regression models for estimating coseismic landslide displacement. Eng Geol 91(2–4):209–218

Keefer DK (2000) Statistical analysis of an earthquake-induced landslide distribution—the 1989 Loma Prieta California event. Eng Geol 58(3–4):231–249

Li MH, Wang DH, Gao YC (2014) Research on the geohazards induced by the M7.9 Luhuo earthquake in Xianshuihe fault zone. J Catastrophol 29(1):37–41

Li Y, Hu KH, Chen XQ, Wei FQ (2006) Characteristic curves and debris flow activity of a valley. J Mt Sci 24(3):320e6

Li ZL, Ba RJ, Ni HY, Liu YJ, Tang YQ, Song Z (2010) Rock mass types and their bearings on the geologic hazards in the Luding region. Sichuan Sediment Geol Tethyan Geol 30(1):103–108

Liu HX, Xu Q, Hou HJ (2013) Influence of lithology and rock structure on slope seismic acceleration responses. Rock and Soil Mech 34(9):2482–2488

Luo Y, Wang Y (2013) Topographic amplification effect of Wenchuan earthquake induced mountain slope vibration. Mountain Res 2:11

Ma Q (1994) Quaternary glaciation on the west slope of Mt. Gongga J Glaciol Geocryol 16(1):6

Mahdavifar MR, Solaymani S (2006) Landslides triggered by the Avaj, Iran earthquake of June 22, 2002. Eng Geol 86(2–3):166–182

Makdisi FI, Seed HB (1978) Simplified procedure for estimating dam and embankment earthquake-induced deformations. J Geotech Eng Div 104(7):849–867

Marc O, Hovius N, Meunier P, Gorum T, Uchida T (2016) A seismologically consistent expression for the total area and volume of earthquake-triggered landsliding. J Geophys Res Earth Surf 121:640–663

Oji S, Kanbara T, Sawada S, Iwata T (2009) Attenuation relationship by considered the effect of directivity based on equivalent hypocentral distance. J Japan Soc Civil Eng Ser. A1 (Struct Eng Earthq Eng (SE/EE)) 65(1):104–110

Pasang S, Kubicek P (2018) Information value model based landslide susceptibility mapping at Phuentsholing, Bhutan. AGILE Conf

Sharma LP, Patel N, Ghose MK, Debnath P (2015) Development and application of Shannon's entropy integrated information value model for landslide susceptibility assessment and zonation in Sikkim Himalayas in India. Nat Hazards 75(2):1555–1576

Shi LB, & Lin CY(1992) Characteristics of fault rocks and fault activities in Kangding Moxi fault zone. Seismol Geol (2). (In Chinese)

Singh O, Sarangi A, Sharma MC (2008) Hypsometric integral estimation methods and its relevance on erosion status of north-western lesser Himalayan watersheds. Water Resour Mgmt 22(11):1545–1560

Strahler AN (1952) Hypsometric (area-altitude) analysis of erosional topography. Geol Soc Am Bull 63(11):1117–1142
Tan-yu X, Xin Y, Yong-shuang Z (2010) A review on study of activity of Xianshuihe fault zone since the Holocene. J Geomech 16(2):176–188
Xiang LZ, Li Y, Chen HK, Su FH, Huang X (2015) Sensitivity analysis of debris flow along highway based on geomorphic evolution theory. Resour Environ Yangtze Basin 24(11):1984–1992
Xiao Z, Xu C, Huang Y, He X, Shao X, Chen Z, Xu X (2023) Analysis of spatial distribution of landslides triggered by the Ms 6.8 Luding earthquake in China on September 5, 2022. Geoenviron Disasters 10(1):1–15
Xu Q (2009). Main types and characteristics of the geohazards triggered by the Wenchuan earthquake. Journal of Geological Hazards and Environment Preservation 20(2):8
Xu Q, Chen JJ. Feng WK, Xiao RH, Zuo YY (2009) Study of the seismic response of slopes by physical modeling. Journal of Sichuan University (Engineering Science Edition). 41(3):266–272
Xu Q, Li WL (2010). Distribution of large-scale landslides induced by the wenchuan earthquake. J Eng Geol 18(6):818–826
Yang CC, Xu HT(2013) Fault rock and fault activity characteristics of Moxi fault zone. Sixth Symp Geol Struct Geodyn (2013):392–392
Yang Z, Liu C, Nie R, Zhang W, Zhang L, Zhang Z, Lu H (2022) Research on uncertainty of landslide susceptibility prediction—bibliometrics and knowledge graph analysis. Remote Sens 14(16):3879
Zhang J, Li Z, Zhang J, Liu X, Ouyang Y (2013) Remote sensing monitoring of geological hazards on Moxi platform in Luding County of Sichuan Province. Bull Soil Water Conserv 33(3):6 (In China)
Zhang JY, Bo JS, Wang ZY, Lin W, Lu T (2012) Influence of local topography on seismic ground motion in Wenchuan earthquake. J Nat Disasters 21(3):164–169
Zheng B (2001) Study on the quaternary glaciation and the formation of the Moxi Platform in the East Slopes of the Mount Gongga. J Glaciol Geocryol 23(3):9

Xuemei Liu · Pengcheng Su · Yong Li
Key Laboratory of Mountain Hazards and Earth Surface Processes, Institute of Mountain Hazards and Environment, Chinese Academy of Sciences, 610000 Chengdu, China

Xuemei Liu · Rui Xu · Dahu Li
Sichuan Earthquake Administration, Chengdu 610041, China

Zhaoxu Xia · Siyuan Ma · Renmao Yuan (✉)
Institute of Geology, China Earthquake Administration, Beijing 100029, China
Email: yuanrenmao@ies.ac.cn

Yao Lu
Shanxi Earthquake Administration, Taiyuan 030021, China

Heng Lu
State Key Laboratory of Hydraulics and Mountain River Engineering, Chengdu 610065, China